



Hutson, C., & Reichmann, M. (2019). New test beam results of 3D and pad detectors constructed with poly-crystalline CVD diamond. *Nuclear Inst. and Methods in Physics Research, A*.  
<https://doi.org/10.1016/j.nima.2019.162675>

Peer reviewed version

License (if available):  
CC BY-NC-ND

Link to published version (if available):  
[10.1016/j.nima.2019.162675](https://doi.org/10.1016/j.nima.2019.162675)

[Link to publication record in Explore Bristol Research](#)  
PDF-document

This is the accepted author manuscript (AAM). The final published version (version of record) is available online via Elsevier at [10.1016/j.nima.2019.162675](https://doi.org/10.1016/j.nima.2019.162675). Please refer to any applicable terms of use of the publisher.







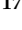









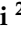
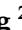





## University of Bristol - Explore Bristol Research

### General rights

This document is made available in accordance with publisher policies. Please cite only the published version using the reference above. Full terms of use are available:  
<http://www.bristol.ac.uk/red/research-policy/pure/user-guides/ebr-terms/>

Article

# A study of the radiation tolerance of CVD diamond to 70 MeV protons, fast neutrons and 200 MeV pions

The RD42 Collaboration: L. Bäni <sup>24,\*</sup> , A. Alexopoulos <sup>3</sup>, M. Artuso <sup>20</sup>, F. Bachmair <sup>24</sup> , M. Bartosik <sup>3</sup>, H. Beck <sup>23</sup>, V. Bellini <sup>2</sup>, V. Belyaev <sup>12</sup>, B. Bentele <sup>19</sup>, A. Bes <sup>27</sup>, J.-M. Brom <sup>7</sup>, G. Chiodini <sup>26</sup>, D. Chren <sup>18</sup>, V. Cindro <sup>9</sup>, G. Claus <sup>7</sup>, J. Collot <sup>27</sup>, J. Cumalat <sup>19</sup>, S. Curtoni <sup>27</sup>, A. Dabrowski <sup>3</sup>, R. D'Alessandro <sup>4</sup>, D. Dauvergne <sup>27</sup>, W. de Boer <sup>10</sup>, C. Dorfer <sup>24</sup> , M. Dünser <sup>3</sup> , G. Eigen <sup>30</sup>, V. Eremin <sup>6</sup>, J. Forneris <sup>15</sup>, L. Gallin-Martel <sup>27</sup>, M.-L. Gallin-Martel <sup>27</sup>, K. K. Gan <sup>13</sup>, M. Gastal <sup>3</sup>, A. Ghimouz <sup>27</sup>, M. Goffe <sup>7</sup>, J. Goldstein <sup>17</sup>, A. Golubev <sup>8</sup>, A. Gorišek <sup>9</sup> , E. Grigoriev <sup>8</sup>, J. Grosse-Knetter <sup>23</sup>, A. Grummer <sup>21</sup>, B. Hiti <sup>9</sup>, D. Hits <sup>24</sup> , M. Hoferkamp <sup>21</sup>, J. Hosselet <sup>7</sup>, F. Hügging <sup>1</sup>, C. Hutton <sup>17</sup>, J. Janssen <sup>1</sup> , H. Kagan <sup>13</sup> , K. Kanxheri <sup>28</sup>, R. Kass <sup>13</sup>, M. Kis <sup>5</sup>, G. Kramberger <sup>9</sup> , S. Kuleshov <sup>8</sup>, A. Lacoste <sup>27</sup> , S. Lagomarsino <sup>4</sup>, A. Lo Giudice <sup>15</sup>, I. López Paz <sup>22</sup>, E. Lukosi <sup>25</sup>, C. Maazouzi <sup>7</sup>, I. Mandić <sup>9</sup>, S. Marcatili <sup>27</sup>, A. Marino <sup>19</sup>, C. Mathieu <sup>7</sup>, M. Menichelli <sup>28</sup>, M. Mikuž <sup>9</sup> , A. Morozzi <sup>28</sup>, F. Moscatelli <sup>28</sup>, J. Moss <sup>29</sup>, R. Mountain <sup>20</sup>, A. Oh <sup>22</sup> , P. Olivero <sup>15</sup>, D. Passeri <sup>28</sup>, H. Pernegger <sup>3</sup> , R. Perrino <sup>26</sup> , F. Picollo <sup>15</sup>, M. Pomorski <sup>11</sup>, R. Potenza <sup>2</sup>, A. Quadt <sup>23</sup>, F. Rarbi <sup>27</sup>, A. Re <sup>15</sup>, M. Reichmann <sup>24</sup> , S. Roe <sup>3</sup>, O. Rossetto <sup>27</sup>, D. A. Sanz Becerra <sup>24</sup> , C. J. Schmidt <sup>5</sup>, S. Schnetzer <sup>14</sup>, S. Sciortino <sup>4</sup>, A. Scorzoni <sup>28</sup>, S. Seidel <sup>21</sup> , L. Servoli <sup>28</sup>, D. S. Smith <sup>13</sup>, B. Sopko <sup>18</sup>, V. Sopko <sup>18</sup>, S. Spagnolo <sup>26</sup>, S. Spanier <sup>25</sup>, K. Stenson <sup>19</sup>, R. Stone <sup>14</sup>, B. Stugu <sup>30</sup>, C. Sutura <sup>2</sup>, M. Traeger <sup>5</sup>, W. Trischuk <sup>16</sup>, M. Truccato <sup>15</sup>, C. Tuvè <sup>2</sup>, J. Velthuis <sup>17</sup>, S. Wagner <sup>19</sup>, R. Wallny <sup>24</sup> , J. C. Wang <sup>20</sup>, N. Wermes <sup>1</sup>, J. Wickramasinghe <sup>21</sup>, M. Yamouni <sup>27</sup>, J. Zalieckas <sup>30</sup>, M. Zavrtanik <sup>9</sup>, K. Hara <sup>32</sup> , Y. Ikegami <sup>31</sup>, O. Jinnouchi <sup>33</sup> , T. Kohriki <sup>31</sup>, S. Mitsui <sup>32</sup> , R. Nagai <sup>33</sup> , S. Terada <sup>31</sup>, Y. Unno <sup>31</sup> 

- 1 Universität Bonn, Bonn, Germany
- 2 INFN/University of Catania, Catania, Italy
- 3 CERN, Geneva, Switzerland
- 4 INFN/University of Florence, Florence, Italy
- 5 GSI, Darmstadt, Germany
- 6 Ioffe Institute, St. Petersburg, Russia
- 7 IPHC, Strasbourg, France
- 8 ITEP, Moscow, Russia
- 9 Jožef Stefan Institute, Ljubljana, Slovenia
- 10 Universität Karlsruhe, Karlsruhe, Germany
- 11 CEA-LIST Technologies Avancées, Saclay, France
- 12 MEPhI Institute, Moscow, Russia
- 13 The Ohio State University, Columbus, OH, USA
- 14 Rutgers University, Piscataway, NJ, USA
- 15 University of Torino, Torino, Italy
- 16 University of Toronto, Toronto, ON, Canada
- 17 University of Bristol, Bristol, UK
- 18 Czech Technical University, Prague, Czech Republic
- 19 University of Colorado, Boulder, CO, USA
- 20 Syracuse University, Syracuse, NY, USA
- 21 University of New Mexico, Albuquerque, NM, USA
- 22 University of Manchester, Manchester, UK
- 23 Universität Göttingen, Göttingen, Germany
- 24 ETH Zürich, Zürich, Switzerland
- 25 University of Tennessee, Knoxville, TN, USA
- 26 INFN-Lecce, Lecce, Italy
- 27 LPSC-Grenoble, Grenoble, France

- 28 INFN-Perugia, Perugia, Italy  
29 California State University, Sacramento, CA, USA  
30 University of Bergen, Bergen, Norway  
31 KEK, High Energy Accelerator Research Organization, Tsukuba, Japan  
32 University of Tsukuba, Tsukuba, Japan  
33 Tokyo Institute of Technology, Tokyo, Japan  
\* Correspondance: lukas.baeni@cern.ch

Version v14 submitted to Sensors

1 **Abstract:** We have measured the radiation tolerance of commercially available diamonds grown  
2 by the Chemical Vapor Deposition process by measuring the charge created by a 120 GeV hadron  
3 beam in a 50  $\mu\text{m}$  pitch strip detector fabricated on each diamond sample before and after irradiation.  
4 We irradiated one group of samples with 70 MeV protons, a second group of samples with fast  
5 reactor neutrons (defined as energy greater than 0.1 MeV) and a third group of samples with  
6 200 MeV pions, in steps, to  $(8.8 \pm 0.9) \times 10^{15}$  protons/cm<sup>2</sup>,  $(1.43 \pm 0.14) \times 10^{16}$  neutrons/cm<sup>2</sup> and  
7  $(6.5 \pm 0.5) \times 10^{14}$  pions/cm<sup>2</sup> respectively. By observing the charge induced due to the separation  
8 of electron-hole pairs created by the passage of the hadron beam through each sample, on an  
9 event-by-event basis, as a function of irradiation fluence, we conclude all data sets can be described  
10 by a first order damage equation and independently calculate the damage constant for 70 MeV  
11 protons, fast reactor neutrons and 200 MeV pions. We find the damage constant for diamond  
12 irradiated with 70 MeV protons to be  $1.61 \pm 0.07$  (stat)  $\pm 0.15$  (syst)  $\times 10^{-18}$  cm<sup>2</sup>/(p  $\mu\text{m}$ ), the damage  
13 constant for diamond irradiated with fast reactor neutrons to be  $2.65 \pm 0.13$  (stat)  $\pm 0.16$  (syst)  $\times$   
14  $10^{-18}$  cm<sup>2</sup>/(n  $\mu\text{m}$ ) and the damage constant for diamond irradiated with 200 MeV pions to be  
15  $2.0 \pm 0.2$  (stat)  $\pm 0.5$  (syst)  $\times 10^{-18}$  cm<sup>2</sup>/( $\pi$   $\mu\text{m}$ ). The damage constants from this measurement were  
16 analyzed together with our previously published 24 GeV proton irradiation and 800 MeV proton  
17 irradiation damage constant data to derive the first comprehensive set of relative damage constants for  
18 Chemical Vapor Deposition diamond. We find 70 MeV protons are  $2.60 \pm 0.27$  times more damaging  
19 than 24 GeV protons, fast reactor neutrons are  $4.27 \pm 0.34$  times more damaging than 24 GeV protons  
20 and 200 MeV pions are  $3.2 \pm 0.8$  more damaging than 24 GeV protons. We also observe the measured  
21 data can be described by a universal damage curve for all proton, neutron and pion irradiations we  
22 have performed of Chemical Vapor Deposition diamond. Finally, we confirm the *FWHM/MP* ratio  
23 of the signal spectrum, a measure of the spatial uniformity of the collected charge, decreases with  
24 fluence for polycrystalline Chemical Vapor Deposition diamond and this effect can also be described  
25 by a universal curve.

26 **Keywords:** Chemical Vapor Deposition; single-crystalline diamond; polycrystalline diamond; charge  
27 collection distance; mean drift path; schubweg; radiation tolerance; radiation damage constant

---

## 28 1. Introduction

29 Diamond-based radiation monitors are now routinely used in high-energy physics experiments  
30 (e.g., at the Large Hadron Collider (LHC) [1]). Their role has become critical in protecting more  
31 sensitive devices against extreme beam conditions and in contributing to a precision measurement of  
32 the luminosity the accelerator delivers. As a result, quantifying the radiation resistance, or damage  
33 constant, of diamond is critical to its use in future upgraded high energy facilities [2,3].

34 In a previously published paper [4] we describe the methodology we used to measure the damage  
35 constants of polycrystalline CVD (pCVD) diamond and single-crystalline CVD (scCVD) diamond  
36 irradiated with 800 MeV and 24 GeV protons. The work described herein uses the same methodology  
37 to measure the damage constants of Chemical Vapor Deposition (CVD) diamond irradiated with  
38 70 MeV protons, fast reactor neutrons with energies greater than 0.1 MeV and 200 MeV pions. In

39 addition, in this manuscript, we derive universal curves for the damage as a function of fluence and the  
40 full width at half maximum divided by its most probable value ( $FWHM/MP$ ) of the signal spectrum  
41 as a function of fluence which may then be used to predict the effects of radiation on any planned  
42 diamond detectors.

## 43 2. Sample Preparation

44 Two types of CVD diamond were used in this work. The first is single-crystalline which, as the  
45 name implies, is ideally one single diamond crystal devoid of grains and grain boundaries. High  
46 purity single-crystalline material has been shown to collect the full charge deposited in the material  
47 but the material area is currently limited to  $\sim 7\text{ mm} \times 7\text{ mm}$ . The second is poly-crystalline which, as  
48 the name implies, is made up of a collection of randomly oriented individual crystal grains and thus  
49 grain boundaries. In poly-crystalline material the collected charge is less than the deposited charge  
50 due to the grain boundaries and their associated dislocations and traps. A high quality,  $500\text{ }\mu\text{m}$  thick,  
51 pCVD diamond collects approximately half of the deposited charge but can be grown in very large  
52 areas up to  $15\text{ cm}$  diameter wafers. In order to quantify the radiation tolerance of scCVD diamond and  
53 pCVD diamond, we used a series of commercially available diamonds for this study [5].

54 In preparing the diamond devices for testing, a  $50\text{ }\mu\text{m}$  pitch strip detector was fabricated on each  
55 sample. The same strip width and strip detector pitch was used for both pCVD and scCVD diamond.  
56 The bias side was fabricated using photolithographic techniques with a single pad. The readout side  
57 was fabricated with photolithographic techniques with  $25\text{ }\mu\text{m}$  wide strips with a  $25\text{ }\mu\text{m}$  gap between  
58 strips producing a device with  $50\text{ }\mu\text{m}$  pitch. The strip pattern was enclosed with a guard ring at the  
59 same potential as the strips to minimize any edge or surface currents from being picked up by the  
60 individual electronic channels. After metalization of both sides with  $500\text{ }\text{\AA}$  Cr and  $2000\text{ }\text{\AA}$  Au, each  
61 device was annealed at  $400\text{ }^\circ\text{C}$  for 4 minutes in an  $\text{N}_2$  atmosphere. The bias electrode side of the device  
62 was attached with silver paint [6] to a ceramic hybrid containing a bias pad and RC bias filter circuit to  
63 power the device. The ceramic hybrid was mounted adjacent to a G-10 printed circuit board which  
64 housed the IDE AS VA2.2 readout chip [7] so each readout strip could be directly wire bonded from  
65 the diamond strip detector to a VA2.2 readout channel.

## 66 3. Sample Description

67 To determine the radiation tolerance of CVD diamond against protons, neutrons and pions seven  
68 samples with different properties were measured before and after irradiation. Two samples were  
69 irradiated with  $70\text{ MeV}$  protons in steps up to a fluence of  $8.8 \times 10^{15}\text{ p/cm}^2$ , two samples were exposed  
70 to fast reactor neutrons up to a fluence of  $14.3 \times 10^{15}\text{ n/cm}^2$  and three samples were irradiated with  
71  $200\text{ MeV}$  pions up to a fluence of  $0.65 \times 10^{15}\text{ }\pi/\text{cm}^2$ . After each irradiation a  $50\text{ }\mu\text{m}$  pitch strip detector  
72 was fabricated on each sample and each device was characterized in a  $120\text{ GeV}$  hadron beam. The  
73 properties of the  $70\text{ MeV}$  proton irradiated samples are listed in Table 1, Table 2 shows the properties of  
74 the fast neutron irradiated samples and Table 3 presents the properties of the pion irradiated samples.  
75 The initial unirradiated signal response of each sample was determined before any irradiations by  
76 fabricating a single pad detector on each diamond sample and measured by using a calibrated setup [8]  
77 with a  $^{90}\text{Sr}$   $\beta$ -source.

## 78 4. Sample Irradiations

### 79 Proton irradiations

80 Samples 1 and 2 were irradiated in the beam course 32 at the CYRIC facility of the Tohoku  
81 University [9]. This facility provided a  $70\text{ MeV}$  proton beam to the beam course in the intensity of  
82  $100\text{ nA}$  to  $1300\text{ nA}$ , with a beam spot size of  $7\text{ mm}$  of full width at half maximum (FWHM). The beam  
83 was scanned over the samples to get a uniform irradiation over the sample area. The particle fluence  
84 for each group of samples irradiated was measured by evaluating the activation of an aluminum foil

**Table 1.** Properties of diamonds irradiated with 70 MeV protons and the fluence they received. The initial unirradiated *ccd* values are given separately for positive and negative bias polarity.

| Diamond Type     | Thickness ( $\mu\text{m}$ ) | Area ( $\text{mm}^2$ ) | Initial <i>ccd</i> ( $\mu\text{m}$ ) | Fluence ( $10^{15} p/\text{cm}^2$ )     |
|------------------|-----------------------------|------------------------|--------------------------------------|---|
| Sample 1<br>pCVD | 518                         | $10 \times 10$         | 227/238                              | 0<br>$8.8 \pm 0.9$                      |
| Sample 2<br>pCVD | 506                         | $10 \times 10$         | 216/216                              | 0<br>$0.96 \pm 0.10$<br>$1.81 \pm 0.18$ |

**Table 2.** Properties of diamonds irradiated with neutrons and the fluence they received. The initial unirradiated *ccd* values are given separately for positive and negative bias polarity.

| Diamond Type     | Thickness ( $\mu\text{m}$ ) | Area ( $\text{mm}^2$ ) | Initial <i>ccd</i> ( $\mu\text{m}$ ) | Fluence ( $10^{15} n/\text{cm}^2$ ) |
|------------------|-----------------------------|------------------------|--------------------------------------|-------------------------------------|
| Sample 3<br>pCVD | 512                         | $5 \times 5$           | 214/204                              | 0<br>$14.3 \pm 1.4$                 |
| Sample 4<br>pCVD | 510                         | $10 \times 10$         | 295/292                              | 0<br>$5.5 \pm 0.5$                  |

**Table 3.** Properties of diamonds irradiated with pions and the fluence they received. The initial unirradiated *ccd* values for the scCVD diamond sample are given separately for positive and negative bias polarity. For samples 6 and 7, only one bias polarity was measured for the unirradiated samples. For these samples the initial *ccd* values are listed for comparison but were not used in the analysis.

| Diamond Type      | Thickness ( $\mu\text{m}$ ) | Area ( $\text{mm}^2$ ) | Initial <i>ccd</i> ( $\mu\text{m}$ ) | Fluence ( $10^{15} \pi/\text{cm}^2$ ) |
|-------------------|-----------------------------|------------------------|--------------------------------------|---------------------------------------|
| Sample 5<br>scCVD | 497                         | $5 \times 5$           | 497/497                              | 0<br>$0.65 \pm 0.14$                  |
| Sample 6<br>pCVD  | 520                         | $5 \times 5$           | 222                                  | 0<br>$0.32 \pm 0.07$                  |
| Sample 7<br>pCVD  | 508                         | $5 \times 5$           | 228                                  | 0<br>$0.61 \pm 0.14$                  |

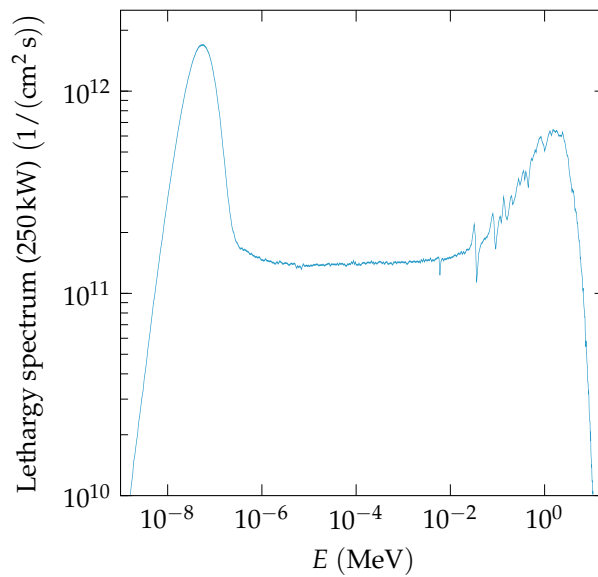
85 for that group of samples irradiated. This method typically measures the dose for each irradiation step  
86 to roughly 10%.

#### 87 Neutron irradiations

88 Samples 3 and 4 were irradiated in channel F19 of core 189 at the TRIGA nuclear reactor of the  
89 Jožef Stefan Institute (JSI) [10] with neutrons. At this facility, the neutron energy spectrum goes from  
90  $10^{-8}$  MeV to 7 MeV [10,11]. The neutron lethargy spectrum ( $\log(E_0/E)$ ) of the F19 channel in core  
91 189 is shown in Fig. 1. Fast neutrons are defined as having an energy greater than 0.1 MeV. The fast  
92 neutron spectrum peaks between 1 MeV and 2 MeV. Fast neutron fluxes up to  $4 \times 10^{12} n/(\text{cm}^2 \text{s})$  are  
93 available and were measured as a function of reactor power using gold foil activation [12]. To measure  
94 the fast neutron accumulated dose, the power of the reactor is set and the exposure time is recorded.  
95 This system typically measures the accumulated dose for each irradiation step to  $\sim 10\%$ .

#### 96 Pion irradiations

97 Samples 5, 6 and 7 were irradiated at PSI [13] with 200 MeV positive pions. Irradiations were  
98 performed by personnel from the CERN IRRAD facility [14]. The fluences were determined at CERN  
99 by measuring the activation in an aluminum foil mounted directly to each sample [15]. In addition to



**Figure 1.** Lethargy neutron spectrum of channel F19 in core 189 of the TRIGA reactor, at full reactor power (250 kW) [11].

100 the statistical error, the CERN IRRAD website quotes an uncertainty of 20 % for these measurements,  
 101 due to the uncertainty on the hardness factor, which was added in quadrature to the statistical error.

## 102 5. Test Beam Analysis

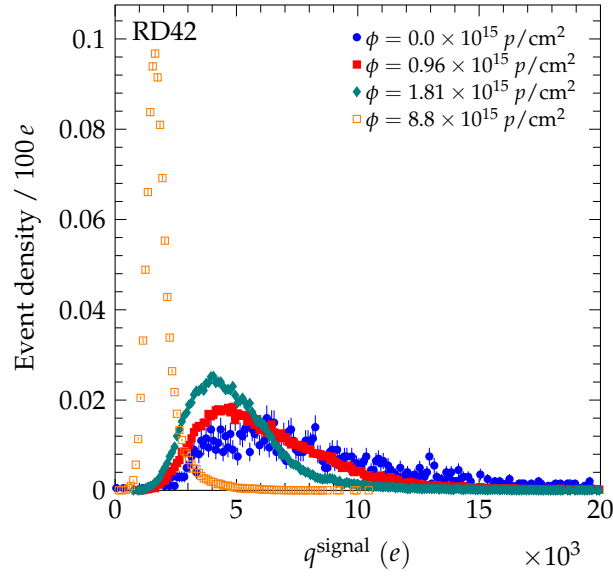
103 The analysis of data in this work uses same analysis procedure and methods described in Ref. [4].  
 104 A brief description is given below and a detailed description can be found in Refs. [16,17].

105 Data from an 8-plane silicon strip telescope [18], based on 50  $\mu\text{m}$  pitch strip detectors with one  
 106 or two floating intermediate strips, were used to reconstruct the predicted particle position in the  
 107 diamond detector to roughly 1.3  $\mu\text{m}$ . A transparent reconstruction algorithm was used to reconstruct  
 108 the signal charge (and actual position) of the particle in the diamond [4]. In this algorithm the charge  
 109 on the highest five contiguous strips within a 500  $\mu\text{m}$  window of the predicted particle position are  
 110 summed to calculate the signal charge and actual position of the particle in the diamond detector.  
 111 In Fig. 2 we present the evolution of the measured signal charge spectrum after the 70 MeV proton  
 112 irradiations. In Fig. 3 the evolution of the measured signal charge spectrum after neutron irradiations is  
 113 shown. In all cases the signal charge spectra get narrower with fluence and the average value decreases  
 114 with fluence. In Fig. 4 the measured signal charge spectrum of an scCVD diamond sensor before and  
 115 after pion irradiation is shown. The average value of the spectrum decreases with fluence. The same  
 116 overall effects were observed previously in the 24 GeV and 800 MeV proton irradiations [4,19].

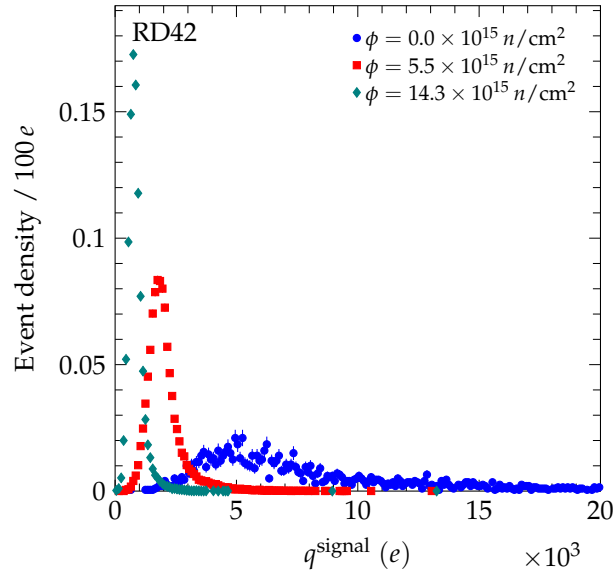
117 The average distance an electron-hole pair drifts apart under the influence of an applied electric  
 118 field or “charge collection distance” ( $ccd$ ) was calculated from the measured signal charge spectrum by

$$ccd = \overline{q^{\text{signal}}} \times \frac{1 \mu\text{m}}{36 e} \quad (1)$$

119 where  $\overline{q^{\text{signal}}}$  is the average of the measured signal charge spectrum in units of  $e$  and  $36 e$  is the average  
 120 number of electron-hole pairs created per micron for a minimum ionizing particle (MIP). We measured  
 121 this quantity by evaluating the signal response of an unirradiated scCVD diamond sample to a  $^{90}\text{Sr}$   
 122  $\beta$ -source. After correcting the electronic gain, offset and deposited charge, we determined the constant  
 123 necessary to collect full charge. This measurement was performed for positive and negative bias  
 124 polarity independently. The unirradiated scCVD diamond used was 497  $\mu\text{m}$  thick. In a measurement  
 125 cycle, we took data at multiple voltages up to  $\pm 500$  V. In the source setup used, the electrons from  $^{90}\text{Sr}$



**Figure 2.** The signal charge spectrum evolution for samples irradiated with 70 MeV protons biased at  $E = +2 \text{ V}/\mu\text{m}$ . The pulse height spectrum before irradiation was measured using a setup with a  $^{90}\text{Sr}$   $\beta$ -source and a single pad metallization on the diamond. The integral of each spectrum has been normalized to unity.



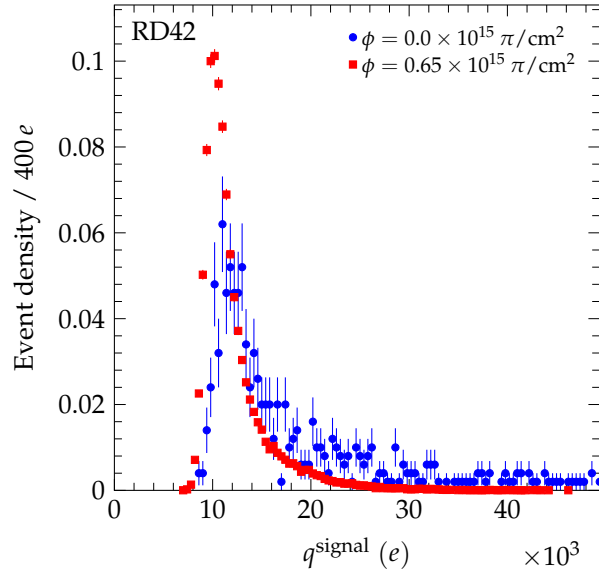
**Figure 3.** The signal charge spectrum evolution for samples irradiated with fast neutrons biased at  $E = -2 \text{ V}/\mu\text{m}$ . The pulse height spectrum before irradiation was measured using a setup with a  $^{90}\text{Sr}$   $\beta$ -source and a single pad metallization on the diamond. The integral of each spectrum has been normalized to unity.

126 are 8 % above minimum ionizing [8]. Our result, after all corrections, is  $(36.0 \pm 0.8) e/\mu\text{m}$  for positive  
 127 bias voltage and  $(35.9 \pm 0.8) e/\mu\text{m}$  for negative bias voltage. These results are consistent with previous  
 128 work [8,20,21]. The *ccd* can be expressed by [22]

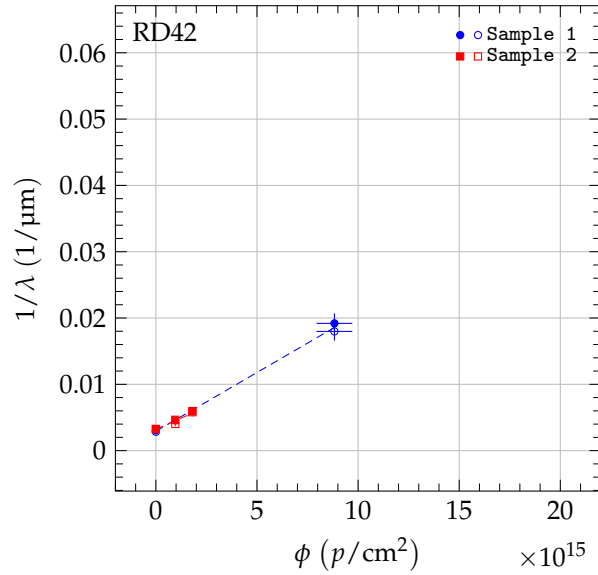
$$\frac{ccd}{t} = \sum_{k=e,h} \frac{\lambda_k}{t} \left[ 1 - \frac{\lambda_k}{t} \left( 1 - e^{-\frac{t}{\lambda_k}} \right) \right] \quad (2)$$

129 where  $t$  is the thickness of the diamond and  $\lambda_k$  is the average distance an electron or hole drifts in  
 130 an infinitely thick sample of a given material. Using (2), the schubweg or average total distance the





**Figure 4.** The signal charge spectrum evolution for the scCVD diamond sample irradiated with 200 MeV pions biased at  $E = +2 \text{ V}/\mu\text{m}$ . The pulse height spectrum before irradiation was measured using a setup with a  $^{90}\text{Sr}$   $\beta$ -source and a single pad metallization on the diamond. The integral of each spectrum has been normalized to unity.



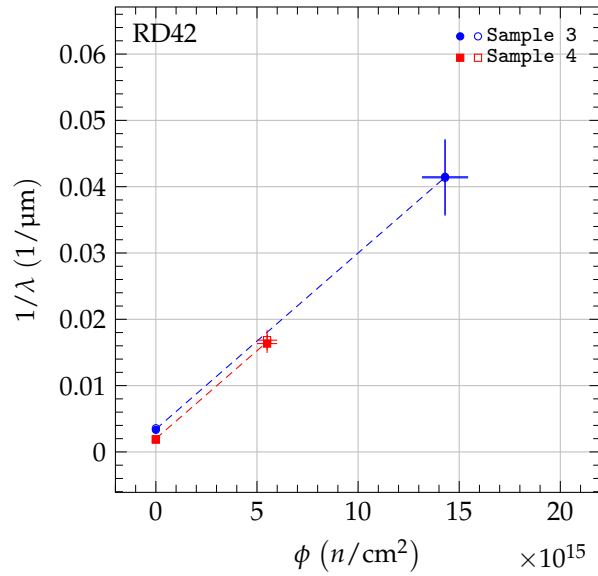
**Figure 5.** The  $1/\lambda$  for pCVD diamond in the 70 MeV proton irradiation. The two values shown at each fluence are the values for positive (solid markers) and negative (open markers) bias at  $E = \pm 2 \text{ V}/\mu\text{m}$ . The data was fit with a first order damage curve independently for each sample.

131 electron-hole pair moves apart, defined as the sum  $\lambda = \lambda_e + \lambda_h$ , was calculated for each beam test  
 132 measurement from the measured  $ccd$ , assuming the ratio  $\lambda_h/\lambda_e = 1.3^{+0.8}_{-0.6}$  [4]. The effect of not knowing  
 133 this ratio exactly was quantified in Ref. [4] and determined to not change the results of this analysis  
 134 within the quoted errors.

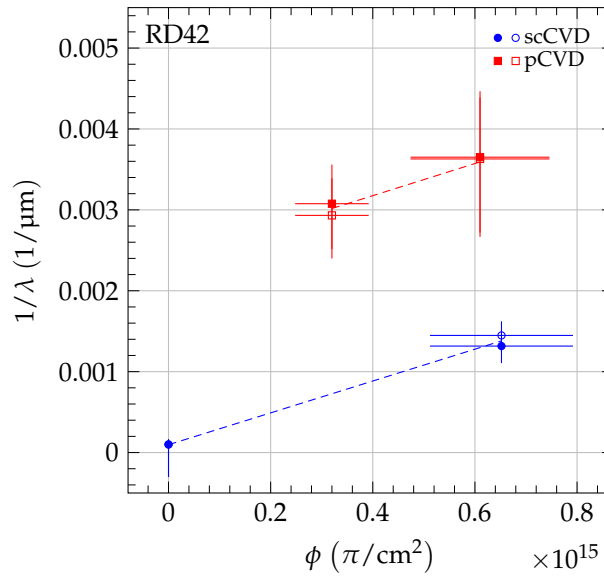
## 135 6. Measurement of Damage Constants

136 After each irradiation step, the diamond devices were characterized in a 120 GeV hadron test  
 137 beam at CERN. In a measurement cycle, the device under test was measured with both positive and  
 138 negative bias voltage to obtain the sum of mean drift paths,  $\lambda$ , for an electric bias field of  $\pm 2 \text{ V}/\mu\text{m}$ .





**Figure 6.** The  $1/\lambda$  for pCVD diamond in the fast neutron irradiation. The two values shown at each fluence are the values for positive (solid markers) and negative (open markers) bias at  $E = \pm 2 \text{ V}/\mu\text{m}$ . The data was fit with a first order damage curve independently for each sample.



**Figure 7.** The  $1/\lambda$  for scCVD and pCVD diamond in the pion irradiation. The two values shown at each fluence are the values for positive (solid markers) and negative (open markers) bias at  $E = \pm 2 \text{ V}/\mu\text{m}$ . The data was fit with a simple damage curve independently for each diamond type. The uncertainty for unirradiated scCVD diamond comes from not knowing the upper initial mean drift distance exactly.

139 A first order damage model was used to describe the irradiation damage effects. The model  
140 relates the inverse sum of mean drift paths,  $1/\lambda$ , linearly with the irradiation fluence by [23]:

$$\frac{1}{\lambda} = \frac{1}{\lambda_0} + k\phi \quad (3)$$

141 where  $k$  is the damage constant and  $\lambda_0$  accounts for charge traps in the unirradiated state. The  
142 inverse sum of mean drift paths as a function of irradiation fluence is shown in Fig. 5 for 70 MeV  
143 proton irradiations, in Fig. 6 for fast neutron irradiations and in Fig. 7 for 200 MeV pion irradiations.  
144 For each sample, the damage model was fitted to the data points to derive the slope. The damage

constant  $k_i$  of particle species  $i$  was derived from the slopes of the individual samples. For the pion irradiated samples, the damage model was fitted separately to the data of scCVD and pCVD diamond samples irradiated with pions and the observed damage constants were combined. The final results of the damage constants for 70 MeV proton irradiations, fast neutron irradiations and 200 MeV pion irradiations are:

$$k_{\text{pCVD}}^{\text{proton}} = 1.61 \pm 0.07 (\text{stat}) \pm 0.15 (\text{syst}) \times 10^{-18} \frac{\text{cm}^2}{p \mu\text{m}}$$

$$k_{\text{pCVD}}^{\text{neutron}} = 2.65 \pm 0.13 (\text{stat}) \pm 0.16 (\text{syst}) \times 10^{-18} \frac{\text{cm}^2}{n \mu\text{m}}$$

$$k^{\text{pion}} = 2.0 \pm 0.2 (\text{stat}) \pm 0.5 (\text{syst}) \times 10^{-18} \frac{\text{cm}^2}{\pi \mu\text{m}}.$$

The general form of the statistical and systematic errors are given in Ref. [4]. Specifically, in this work, the statistical errors are dominated by the error in the fits while the systematic errors are dominated by the signal calibration, the pulse height dependence on track position and the pulse height dependence on bias polarity.

In Table 4 the relative damage constants are compared to the 24 GeV proton and 800 MeV proton results from Ref. [4]. 70 MeV protons are found to be more than twice as damaging as 24 GeV protons, fast reactor neutrons were observed to be more than four times more damaging than 24 GeV protons and 200 MeV pions are more than three times as damaging as 24 GeV protons. These results are roughly consistent with displacement per atom (DPA) [24].

**Table 4.** Relative damage constants for 24 GeV protons, 800 MeV protons, 70 MeV protons, 200 MeV pions and fast reactor neutrons. The radiation damage constants of 24 GeV protons and 800 MeV protons are from Ref. [4]. The relative radiation damage constant of 25 MeV protons is derived from Ref. [25].

| Particle species | $\kappa$        |
|------------------|-----------------|
| 24 GeV protons   | 1.0             |
| 800 MeV protons  | $1.67 \pm 0.09$ |
| 70 MeV protons   | $2.60 \pm 0.27$ |
| 25 MeV protons   | $4.4 \pm 1.2$   |
| Fast neutrons    | $4.27 \pm 0.34$ |
| 200 MeV pions    | $3.2 \pm 0.8$   |

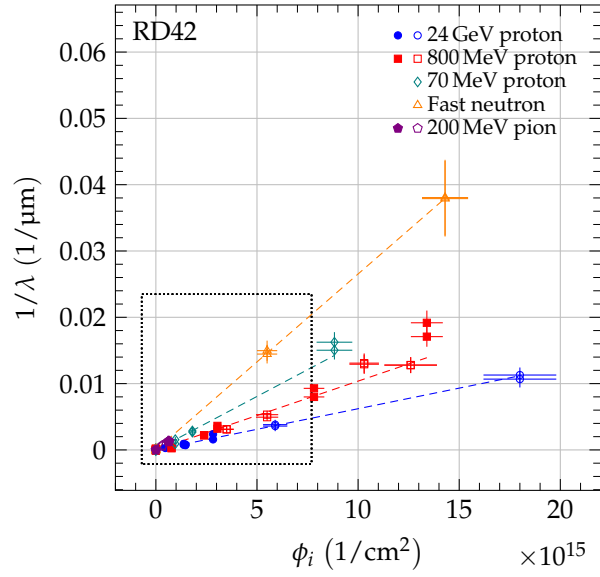
158

## 159 7. Universal Damage Curve

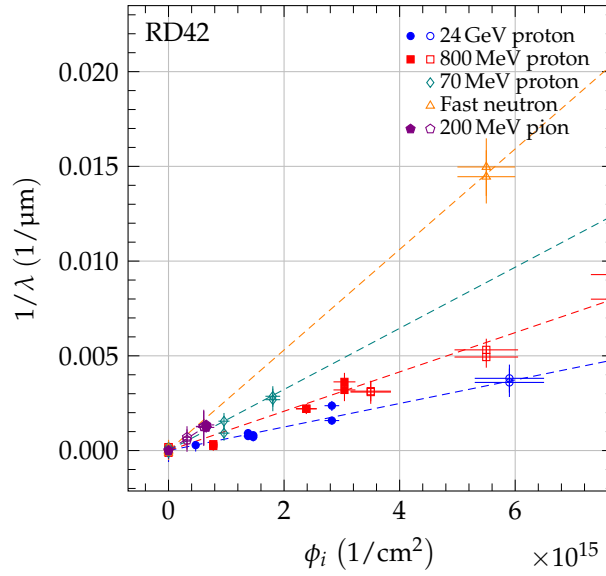
As shown in Ref. [4], scCVD and pCVD diamond follow the same damage model. However, the damage curve of species  $i$  for each diamond sample  $j$  starts at a different values of  $1/\lambda_{0,j}$ , due to the initial collection distance of the sample. The initial  $\lambda_{0,j}$  of sample  $j$  was derived by fitting a slope equal to the damage constant  $k_i$  to the data points. Table 5 lists the parameter  $\lambda_{0,j}$  of the tested samples. In Fig. 8, the  $1/\lambda$  as a function of fluence for 70 MeV proton, fast neutron and 200 MeV pion irradiations is compared to the result of 24 GeV proton and 800 MeV proton irradiations [4] with the data points shifted by  $1/\lambda_{0,j}$ . The difference in slope of the dashed lines in this figure reflects the difference in damage constants. Fig. 9 shows the data from Fig. 8 in the dotted box to illustrate the relation of the low fluence data and the damage curves.

Since scCVD and pCVD diamond follow the same damage model in (3) and different irradiations have different shift, it should be possible to generate a universal damage curve. To accomplish this the fluences were scaled by

$$\phi_{24\text{ GeV } p \text{ eq}} = \kappa_i \times \phi_i \quad (4)$$



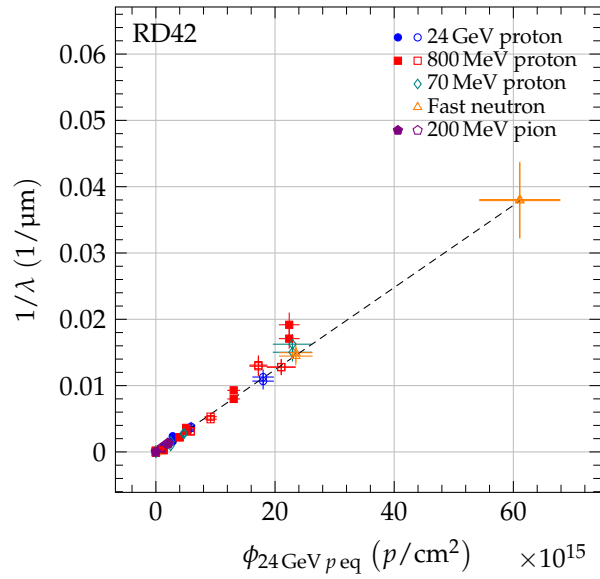
**Figure 8.** The  $1/\lambda$  for scCVD (solid markers) and pCVD (open markers) diamond. As reference the 800 MeV proton and 24 GeV proton data from Ref. [4] are plotted. Each pCVD point is shifted by  $1/\lambda_{0,i}$ . The dotted box indicates the zoom area shown in Fig. 9.



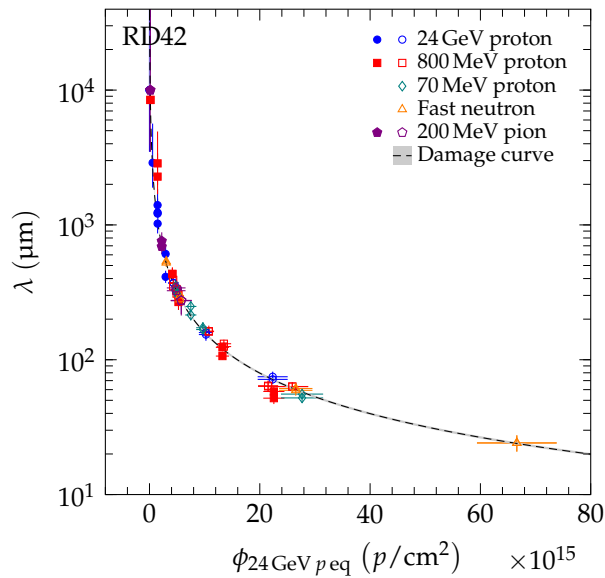
**Figure 9.** The  $1/\lambda$  for scCVD (solid markers) and pCVD (open markers) diamond up to a fluence of  $7 \times 10^{15}/\text{cm}^2$  (zoom of dotted box in Fig. 8). As reference the 800 MeV proton and 24 GeV proton data from Ref. [4] are plotted. Each pCVD point is shifted by  $1/\lambda_{0,i}$ .

**Table 5.** Parameter  $\lambda_{0,j}$  and fluence offset  $\phi_{0,j}$  of diamond sample  $j$  for 70 MeV protons, fast reactor neutrons and 200 MeV pions. The derived  $\lambda_{0,j}$  is not universal since it is sample dependent.

| Diamond $j$ | $\lambda_{0,j}$ ( $\mu\text{m}$ ) | $\phi_{0,j}$ ( $10^{15}/\text{cm}^2$ ) |
|-------------|-----------------------------------|--|
| Sample 1    | $339 \pm 21$                      | $4.7 \pm 0.6$                          |
| Sample 2    | $322 \pm 15$                      | $5.0 \pm 0.6$                          |
| Sample 3    | $291 \pm 21$                      | $5.5 \pm 0.7$                          |
| Sample 4    | $531 \pm 27$                      | $3.0 \pm 0.4$                          |
| Sample 5    | $11\,000 \pm 20\,000$             | $0.15 \pm 0.29$                        |
| Sample 6+7  | $420 \pm 60$                      | $3.8 \pm 0.7$                          |



**Figure 10.** The  $1/\lambda$  for scCVD (solid markers) and pCVD (open markers) diamond. Each pCVD point is shifted by  $1/\lambda_{0,i}$ . The fluence of each point was scaled by the relative damage constant,  $\kappa_i$ , to the 24 GeV proton equivalent fluence. The damage model (dashed line) is fitted to the data points.



**Figure 11.** The  $\lambda$  for scCVD (solid markers) and pCVD (open markers) diamond. The fluence of each point was scaled by the relative damage constant to the 24 GeV proton equivalent fluence. Each point is shifted by  $\phi_{0,j}$  which represents the starting value of sample  $j$  in 24 GeV proton equivalent fluence space. The dashed line is the fit of the damage model in (3) to the data points. The gray band indicates the variation of the fit parameters by one standard deviation.

172 where  $\kappa_i$  is the relative radiation damage constant defined as  $\kappa_i = k_i/k_{24\text{GeV}p}$ . The measured  $1/\lambda$  as a  
 173 function of 24 GeV proton equivalent fluence is shown in Fig. 10 and illustrates the universality of the  
 174 first order radiation damage model described above.

175 Instead of the offset  $1/\lambda_{0,j}$ , the separation of the damage curve of species  $i$  for individual diamond  
 176 samples may be interpreted as a fluence offset,  $\phi_{0,j}$ . Thus the initial signal response of pCVD diamond

177 corresponds to irradiated scCVD diamond. The fluence offset in units of 24 GeV proton equivalent  
178 fluence of each diamond sample was calculated using:

$$\phi_{0,j} = \frac{\kappa_i}{\lambda_{0,j}k_i} = \frac{1}{\lambda_{0,j}k_{24\text{GeV}p}} \quad (5)$$

179 where  $k_i$  is the damage constant for particle species  $i$  and  $\lambda_{0,j}$  the initial sum of mean drift paths of  
180 sample  $j$  derived from the fit to the data points of sample  $j$  with fixed  $k_i$ . The fluence offset  $\phi_{0,j}$  is  
181 listed in Table 5. To facilitate predictions of the signal response as a function of particle fluence, the  
182 measured  $\lambda$  of the five data sets were plotted as a function of 24 GeV proton equivalent fluence. To  
183 obtain a universal curve the fluence of species  $i$  was scaled as in (4) and each diamond data point was  
184 shifted by the fluence offset  $\phi_{0,j}$ . The measured  $\lambda$  as a function of 24 GeV proton equivalent fluence of  
185 the data is presented in Fig. 11.

## 186 8. Measurement of the *FWHM/MP* Ratio

187 The initial non-uniformities in unirradiated pCVD material are mainly due to the interior crystal  
188 structure where single grains have different charge collection properties causing a spatial variation  
189 of the Landau-like distributions in the material [19]. This effect was clearly demonstrated in Ref. [4]  
190 where we showed the quantity  $R$ ,

$$R = \frac{FWHM}{MP}, \quad (6)$$

191 is also a measure of the uniformity of the material. The smaller the quantity  $R$  the narrower the  
192 normalized signal charge distribution is across the material. Here we use the full width at half  
193 maximum, *FWHM*, normalized by the most probable value, *MP*, of the signal response [4] to analyze  
194 its irradiation dependence.<sup>1</sup> In order to compare with previous beam test results for  $R$  we used a  
195 +120 GeV/c hadron beam, which are near minimum ionizing, as we did previously [4].

196 The results of the 70 MeV proton irradiations are shown in Fig. 12. The results of the neutron  
197 irradiations are presented in Fig. 13. The value  $R$  decreases for both irradiation species as a function  
198 of fluence, confirming the observation with pCVD diamond in Ref. [4]. The value  $R$  as a function of  
199 200 MeV pion fluence is shown in Fig. 14 and is compatible with the findings in Ref. [4].

200 To compare the results of the different particle species, the fluence of each data point was scaled to  
201 24 GeV proton equivalent fluence using (4). In Fig. 15 the value  $R$  of the five data sets (24 GeV protons,  
202 800 MeV protons, 70 MeV protons, 200 MeV pions and fast neutrons) is shown as a function of 24 GeV  
203 proton equivalent fluence. The pCVD data points all fall on a single curve which decreases with  
204 fluence. The scCVD data all fall on a different curve which is compatible with being flat with fluence.  
205 This is illustrated in Fig. 16 where scCVD diamond data are shown in blue and pCVD diamond data  
206 are shown in red. The two curves taken together indicate the pCVD samples are becoming more  
207 uniform with irradiation and approaching the uniformity of single-crystal diamond.

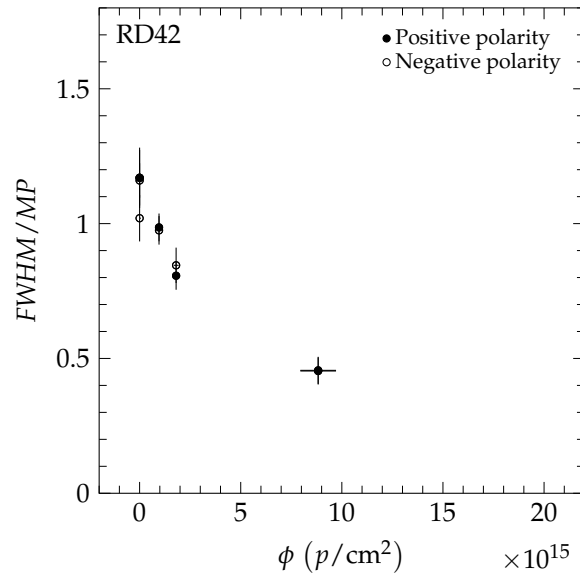
## 208 9. Comparison with Silicon

209 Once the damage constants are determined, the damage constants for diamond may be compared  
210 with the damage constants for silicon. The collected charge in silicon devices depends on the electric  
211 field and trapping times. The trapping time  $\tau_i$  at a temperature  $T$  and time after irradiation,  $t$ , is  
212 inversely proportional to the fluence [26,27]:

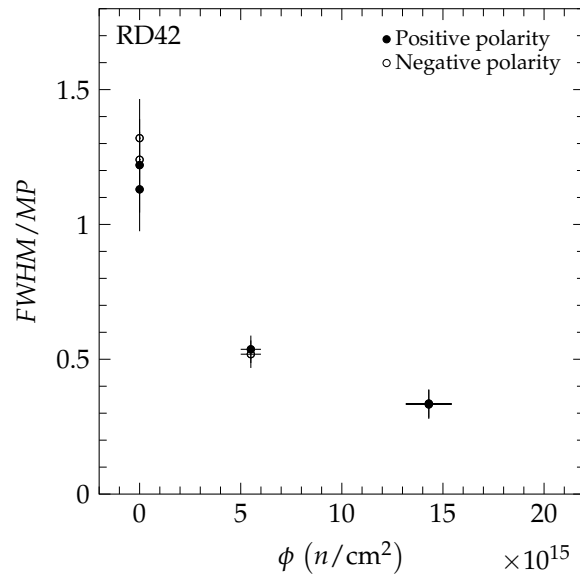
$$\frac{1}{\tau_i} = \beta_i(T, t) \times \phi. \quad (7)$$

---

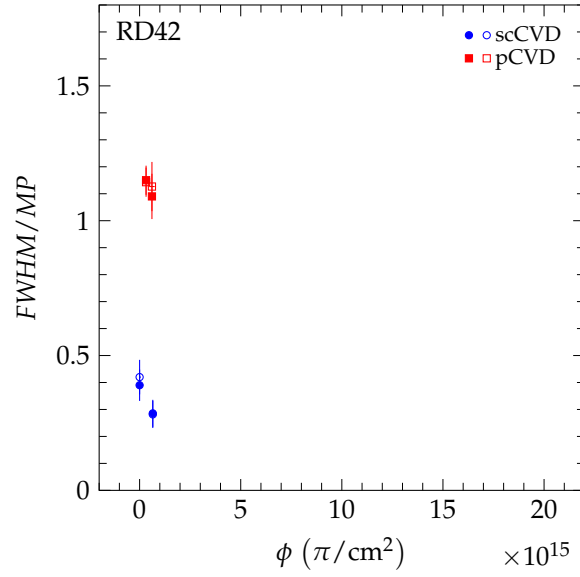
<sup>1</sup> We normalized to *MP*, since the inherent distribution is Landau-like and for Landau distributions the measured mean depends on the number of events attained.



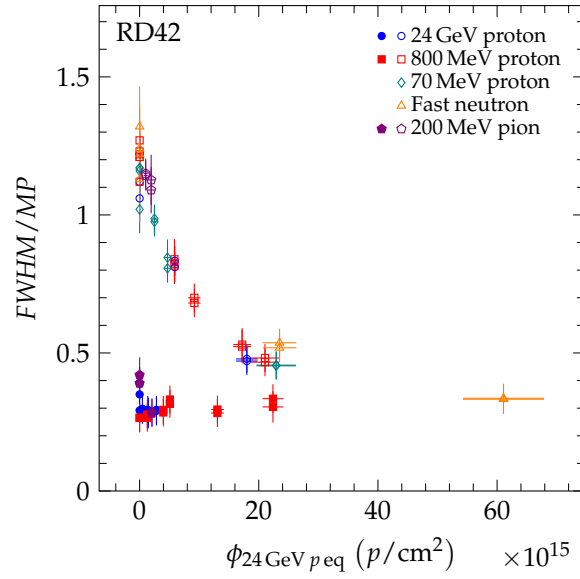
**Figure 12.** The  $FWHM/MP$  as a function of fluence in the 70 MeV proton irradiation measured in a +120 GeV/ $c$  hadron beam at CERN. The two values shown at each fluence are the values for positive (solid markers) and negative bias (open markers) at  $E = 2 \text{ V}/\mu\text{m}$ .



**Figure 13.** The  $FWHM/MP$  as a function of fluence in the fast neutron irradiation measured in a +120 GeV/ $c$  hadron beam at CERN. The two values shown at each fluence are the values for positive (solid markers) and negative bias (open markers) at  $E = 2 \text{ V}/\mu\text{m}$ .



**Figure 14.** The  $FWHM/MP$  as a function of fluence in the pion irradiation measured in a +120 GeV/ $c$  hadron beam at CERN. The two values shown at each fluence are the values for positive (solid markers) and negative bias (open markers) at  $E = 2 \text{ V}/\mu\text{m}$ .



**Figure 15.** The  $FWHM/MP$  for scCVD (solid markers) and pCVD (open markers) diamond. The fluence of each point was scaled by the relative damage constant to the 24 GeV proton equivalent fluence.

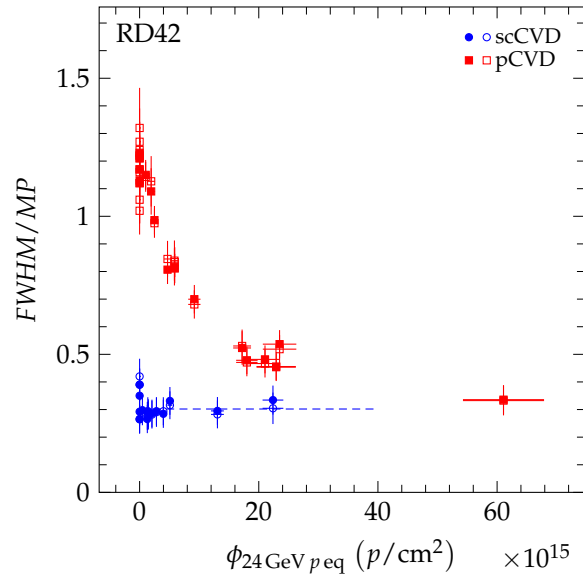
213 From the measurements of trapping times which require a fully depleted detector, the mean drift path  
214 of the charge carriers,  $\lambda$ , may be calculated using the relation

$$\lambda = v_e \tau_e + v_h \tau_h \quad (8)$$

215 where  $v_i$  are the drift velocities of electrons and holes, respectively. Using (7) and (8),  $1/\lambda$  as a function  
216 of fluence for silicon may be described by

$$\frac{1}{\lambda} = \frac{1}{\frac{v_e}{\beta_e} + \frac{v_h}{\beta_h}} \times \phi = k\phi \quad (9)$$





**Figure 16.** The  $FWHM/MP$  of scCVD and pCVD diamond samples irradiated with 24 GeV protons, 800 MeV protons, 70 MeV protons and fast reactor neutron for positive (solid markers) and negative bias (open markers) at  $E = 2 \text{ V}/\mu\text{m}$ . The fluence of each point was scaled by the relative damage constant to the 24 GeV proton equivalent fluence. The dashed line represents a constant fit to the scCVD diamond data points (blue) extrapolated to  $40 \times 10^{15} \text{ p}/\text{cm}^2$  for illustrative purposes.

217 where  $k$  is a damage constant.

218 In Fig. 17 the damage constants measured at an electric field of  $2 \text{ V}/\mu\text{m}$  and at  $T = 20^\circ\text{C}$  for  
 219 diamond and silicon were used to generate the inverse sum of mean drift paths versus fluence plot  
 220 up to a fluence of  $10^{15} \text{ particles}/\text{cm}^2$ . The dashed lines are the diamond results from this work and  
 221 Ref. [4] for the irradiations of 24 GeV protons (blue), 800 MeV protons (red), 70 MeV protons (green),  
 222 200 MeV pions (purple) and fast neutrons (orange). The solid lines are the silicon data from RD50 [28]  
 223 for proton (blue and red), pion (purple) and neutron (orange) irradiations. The sum of mean drift  
 224 paths is obtained from charge collection measurements at room temperature, assuming a uniform  
 225 electric field of  $2 \text{ V}/\mu\text{m}$ . Drift velocities at  $2 \text{ V}/\mu\text{m}$  were derived from Ref. [29] and trapping times  
 226 were taken from Ref. [27] after 80 min of annealing at  $60^\circ\text{C}$ .

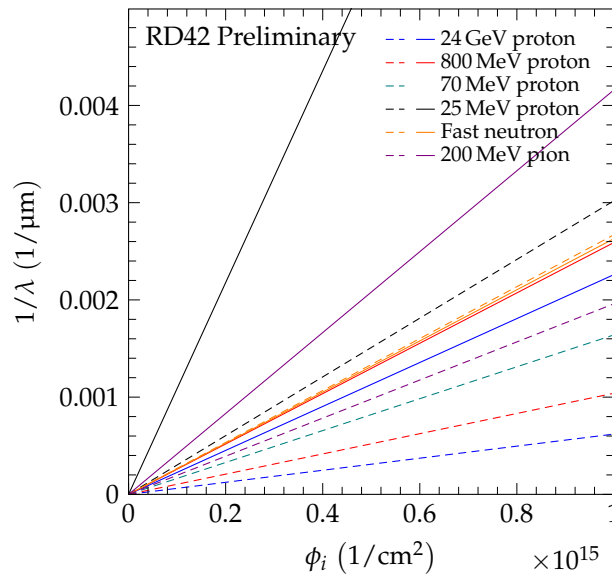
227 The results from Fig. 17 show that for proton irradiations diamond is much less radiation sensitive  
 228 than silicon (greater than a factor of two) for all proton energies while for neutron irradiations silicon  
 229 is comparable in radiation tolerance to diamond.

## 230 10. Summary

231 A study of CVD diamond material before and after a series of irradiations with 70 MeV protons,  
 232 fast reactor neutrons and 200 MeV pions is presented. The decrease in signal response is in agreement  
 233 with a first order damage model. The measured data have been compared to previous measurements  
 234 of CVD diamond samples irradiated with 800 MeV protons and 24 GeV protons [4]. Furthermore, the  
 235 five data sets have been combined in a universal damage curve for diamond material which allows  
 236 predictions to be made for potential applications.

237 The decrease in  $FWHM/MP$  of the signal response of the collected charge as a function of particle  
 238 fluence has been confirmed for pCVD diamond material irradiated with 70 MeV protons and fast  
 239 reactor neutrons. Moreover, the measurements of this paper have been combined with previous  
 240 measurements [4] into a universal curve.

241 Finally, the radiation damage constants of diamond have been compared to the radiation damage  
 242 constants of silicon. For proton irradiations, diamond has been found to be more radiation tolerant  
 243 than silicon, while a comparable radiation tolerance against neutrons has been observed.



**Figure 17.** The  $1/\lambda$  for CVD diamond and silicon for proton, pion and neutron irradiations at an electric field of  $2\text{ V}/\mu\text{m}$ . The charge collection was measured at room temperature. The dashed lines are diamond results from this work and Ref. [4] for irradiations at 24 GeV protons (blue), 800 MeV protons (red), 70 MeV protons (green) and fast neutrons (orange) and the solid lines are the silicon damage data from RD50 [28] for proton (blue and red), pion (purple) and neutron (orange) irradiations. The curves for irradiations with 25 MeV protons were taken from Ref. [25].

244 **Author Contributions:** Software, F. Bachmair, L. Bäni, G. Claus, M. Goffe, M. Reichmann, D. A. Sanz Becerra,  
 245 R. Wallny; Formal Analysis, F. Bachmair, L. Bäni, D. Hits, H. Kagan, G. Kramberger, M. Mikuž, A. Oh,  
 246 W. Trischuk; Investigation, A. Alexopoulos, M. Artuso, F. Bachmair, L. Bäni, M. Bartosik, H. Beck, V. Bellini,  
 247 B. Bentele, A. Bes, J.-M. Brom, G. Chiodini, V. Cindro, G. Claus, J. Collot, J. Cumalat, S. Curtoni, A. Dabrowski,  
 248 R. D’Alessandro, D. Dauvergne, W. de Boer, C. Dorfer, M. Dünser, G. Eigen, V. Eremin, J. Forneris, L. Gallin-Martel,  
 249 M.-L. Gallin-Martel, K. K. Gan, M. Gastal, A. Ghimouz, M. Goffe, J. Goldstein, A. Golubev, A. Gorišek, E. Grigoriev,  
 250 J. Grosse-Knetter, A. Grummer, B. Hiti, D. Hits, M. Hoferkamp, J. Hosselet, F. Hügging, C. Hutton, J. Janssen,  
 251 H. Kagan, K. Kanxheri, R. Kass, M. Kis, G. Kramberger, S. Kuleshov, A. Lacoste, S. Lagomarsino, A. Lo Giudice,  
 252 I. López Paz, E. Lukosi, C. Maazouzi, I. Mandić, S. Marcatili, A. Marino, C. Mathieu, M. Menichelli, M. Mikuž,  
 253 A. Morozzi, F. Moscatelli, J. Moss, R. Mountain, A. Oh, P. Olivero, D. Passeri, H. Pernegger, R. Perrino, F. Picollo,  
 254 R. Potenza, A. Quadt, F. Rarbi, A. Re, S. Roe, O. Rossetto, D. A. Sanz Becerra, C. J. Schmidt, S. Schnetzer,  
 255 S. Sciortino, A. Scorzoni, S. Seidel, L. Servoli, D. S. Smith, S. Spagnolo, S. Spanier, K. Stenson, R. Stone, B. Stugu,  
 256 C. Sutura, M. Traeger, W. Trischuk, M. Truccato, C. Tuvè, J. Velthuis, S. Wagner, R. Wallny, J. C. Wang, N. Wermes,  
 257 J. Wickramasinghe, M. Yamouni, J. Zalieckas, M. Zavrtanik, K. Hara, Y. Ikegami, O. Jinnouchi, T. Kohriki, S. Mitsui,  
 258 R. Nagai, S. Terada, Y. Unno; Data Curation, F. Bachmair, L. Bäni, M. Goffe, A. Gorišek, D. Hits, J. Janssen,  
 259 H. Kagan, G. Kramberger, A. Oh, M. Reichmann, D. A. Sanz Becerra, S. Seidel, R. Wallny, K. Hara, Y. Ikegami,  
 260 O. Jinnouchi, T. Kohriki, S. Mitsui, R. Nagai, S. Terada, Y. Unno; Writing, F. Bachmair, L. Bäni, D. Hits, H. Kagan,  
 261 G. Kramberger, A. Oh, W. Trischuk; Supervision, M. Artuso, W. de Boer, J.-M. Brom, G. Chiodini, G. Eigen,  
 262 V. Eremin, M.-L. Gallin-Martel, J. Goldstein, A. Golubev, F. Hügging, H. Kagan, M. Kis, M. Mikuž, J. Moss,  
 263 A. Oh, P. Olivero, H. Pernegger, R. Potenza, A. Quadt, S. Schnetzer, S. Sciortino, S. Seidel, L. Servoli, S. Spanier,  
 264 W. Trischuk, C. Tuvè, S. Wagner, R. Wallny, N. Wermes; Project Administration, H. Kagan, W. Trischuk; Funding  
 265 Acquisition, J.-M. Brom, J. Goldstein, H. Kagan, M. Mikuž, J. Moss, A. Oh, H. Pernegger, A. Quadt, S. Seidel,  
 266 S. Schnetzer, W. Trischuk, R. Wallny, N. Wermes, K. Hara, S. Terada, Y. Unno

267 **Funding:** The research leading to these results received funding from the European Union’s Horizon 2020 research  
 268 and innovation program under grant agreement No. 654168. This work was also partially supported by the  
 269 Swiss National Science Foundation grant #20FL20\_154216, ETH grant 51 15-1, Swiss Government Excellence  
 270 Scholarship ESKAS No. 2015.0808, UK Science and Technology Facilities Council grant ST/M003965/1 and the  
 271 U.S. Department of Energy through grant DE-SC0011726.

272 **Acknowledgments:** The RD42 Collaboration gratefully acknowledges the staff at CERN for test beam time, their  
 273 help in setting up the beam conditions and for their assistance in making our tests a success. We would also like  
 274 to thank Profs. T. Shinozuka, T. Wakui, and the staff of the CYRIC Irradiation Facility at Tohoku University in  
 275 Sendai, Japan for their help in the 70 MeV proton irradiations (experiments 8705 and 9214) and the staff of the  
 276 TRIGA Nuclear Reactor at the Jožef Stefan Institute in Ljubljana, Slovenia for their help in making the neutron  
 277 irradiations possible.

278 **Conflicts of Interest:** The authors declare no conflicts of interest.

## 279 References

- 280 1. CERN The European Organization for Nuclear Research, CH-1211, Genève 23, Switzerland. For additional  
281 information see: <https://home.cern/>.
- 282 2. G. Apollinari *et al.*, "High-Luminosity Large Hadron Collider (HL-LHC): Preliminary Design Report, Chapter  
283 1: High-Luminosity Large Hadron Collider HL-LHC," CERN Yellow Reports: Monographs, CERN-2015-005,  
284 CERN Geneva, 2015; DOI: [10.5170/CERN-2015-005.1](https://doi.org/10.5170/CERN-2015-005.1).
- 285 3. G. Apollinari *et al.*, "High-Luminosity Large Hadron Collider (HL-LHC): Technical Design Report  
286 V.0.1," CERN Yellow Reports: Monographs, Volume 4/2017 CERN-2017-007-M, CERN Geneva 2017;  
287 DOI: [10.23731/CYRM-2017-004](https://doi.org/10.23731/CYRM-2017-004).
- 288 4. L. Băni, *et al.* [RD42 Collaboration], "A study of the radiation tolerance of poly-crystalline and  
289 single-crystalline CVD diamond to 800 MeV and 24 GeV protons," J. Phys. D: Appl. Phys. **52**, 465103  
290 (2019); DOI: [10.1088/1361-6463/ab37c6](https://doi.org/10.1088/1361-6463/ab37c6).
- 291 5. The samples used in this study were electronic grade CVD diamond purchased from Element Six  
292 Technologies, Global Innovation Centre, Fermi Ave., Harwell, OX11 0QR, United Kingdom. and II-VI  
293 Incorporated, 375 Saxonburg Blvd., Saxonburg, PA 16056-9499, USA. URL <http://www.iivinfrared.com>.
- 294 6. Dotite silver paint D-550. Fujikura Kasei Co., LTD. 6-15, Shibakoen 2-chome, Minato-ku, Tokyo 105-0011  
295 Japan; TEL. 81-3-3436-1100 <https://www.fkkasei.co.jp/english/product/electric/dotite/05.html>
- 296 7. Integrated Detector and Electronics (IDE) AS designed the VA circuits. <http://www.ideas.no>.
- 297 8. S. Zhao, "Characterization of the electrical properties of polycrystalline diamond films," Ph.D. Thesis, The  
298 Ohio State University, (1994); URL: [http://rave.ohiolink.edu/etdc/view?acc\\_num=osu1394810346](http://rave.ohiolink.edu/etdc/view?acc_num=osu1394810346).
- 299 9. Cyclotron and Radioisotope Center (CYRIC), Tohoku University, Sendai, Miyagi, Japan. For additional  
300 information see: <http://www.cyric.tohoku.ac.jp>.
- 301 10. L. Snoj, G. Žerovnik and A. Trkov, "Computational analysis of irradiation facilities at the JSI TRIGA reactor,"  
302 Appl. Radiat. Isot. **70**, 483 (2012); DOI: [10.1016/j.apradiso.2011.11.042](https://doi.org/10.1016/j.apradiso.2011.11.042).
- 303 11. K. Ambrožič, G. Žerovnik and L. Snoj, "Computational analysis of the dose rates at JSI TRIGA reactor  
304 irradiation facilities," Appl. Radiat. Isot. **130**, 140 (2017); DOI: [10.1016/j.apradiso.2017.09.022](https://doi.org/10.1016/j.apradiso.2017.09.022).
- 305 12. E. S. Krištof, "Characterization of neutron flux in the exposure channel F19 of the TRIGA Mark II reactor in  
306 Ljubljana," Nuclear Energy in Central Europe '98. 43 (1998).
- 307 13. Paul Scherrer Institute (PSI), 5232 Villigen, Switzerland. <https://www.psi.ch>.
- 308 14. CERN IRRAD proton facility, <https://ps-irrad.web.cern.ch/ps-irrad/external.php>.
- 309 15. M. Glaser, F. Ravotti and M. Moll, "Dosimetry assessments in the irradiation facilities at the CERN-PS  
310 accelerator," IEEE Trans. Nucl. Sci. **53**, 2016–2022 (2006); DOI: [10.1109/TNS.2006.880569](https://doi.org/10.1109/TNS.2006.880569).
- 311 16. F. Bachmair, "CVD Diamond Sensors in Detectors for High Energy Physics," Ph.D. Thesis, ETH Zürich,  
312 (2016); DOI: [10.3929/ethz-a-010748643](https://doi.org/10.3929/ethz-a-010748643).
- 313 17. L. Băni, "Top Quarks and Diamonds," Ph.D. Thesis, ETH Zürich, (2017); DOI: [10.3929/ethz-b-000222412](https://doi.org/10.3929/ethz-b-000222412).
- 314 18. C. Colledani *et al.*, "A Submicron Precision Silicon Telescope for Beam Test Purposes," Nucl. Instr. and Meth.  
315 A **372**, 379 (1996); DOI: [10.1016/0168-9002\(95\)01414-4](https://doi.org/10.1016/0168-9002(95)01414-4).
- 316 19. D. Meier, "CVD Diamond Sensors for Particle Detection and Tracking," Ph.D. Thesis, Universität Heidelberg,  
317 (1999).
- 318 20. L. S. Pan *et al.*, "Particle- and photoinduced conductivity in type-IIa diamonds," J. Appl. Phys. **74**, 1086  
319 (1993); DOI: [10.1063/1.354957](https://doi.org/10.1063/1.354957).
- 320 21. M. Muškinja *et al.*, "Investigation of charge multiplication in single crystalline CVD diamond," Nucl. Instr.  
321 and Meth. A **841**, 162 (2017); DOI: [10.1016/j.nima.2016.10.018](https://doi.org/10.1016/j.nima.2016.10.018).
- 322 22. K. Hecht, "Zum Mechanismus des lichtelektrischen Primärstromes in isolierenden Kristallen," Z. Phys. **77**,  
323 235 (1932); DOI: [10.1007/BF01338917](https://doi.org/10.1007/BF01338917).
- 324 23. F. Hartjes *et al.* [RD42 Collaboration], "Parameterisation of Radiation Effects on CVD Diamond for Proton  
325 Irradiation," Nucl. Phys. B (Proc. Suppl.) **78**, 675 (1999); DOI: [10.1016/S0920-5632\(99\)00623-4](https://doi.org/10.1016/S0920-5632(99)00623-4).
- 326 24. M. Guthoff, W. de Boer and S. Müller, "Simulation of beam induced lattice defects of diamond detectors  
327 using FLUKA," Nucl. Instr. and Meth. A **735**, 223 (2014); DOI: [10.1016/j.nima.2013.08.083](https://doi.org/10.1016/j.nima.2013.08.083).

- 328 25. J.-W. Tsung *et al.*, "Signal and noise of diamond pixel detectors at high radiation fluences," JINST 7 (2012)  
329 P09009; DOI: [10.1088/1748-0221/7/09/P09009](https://doi.org/10.1088/1748-0221/7/09/P09009).
- 330 26. G. Kramberger, V. Cindro, I. Mandić, M. Mikuž and M. Zavrtanik, "Determination of effective trapping  
331 times for electrons and holes in irradiated silicon," Nucl. Instr. and Meth. A 476, 645 (2002);  
332 DOI: [10.1016/S0168-9002\(01\)01653-9](https://doi.org/10.1016/S0168-9002(01)01653-9).
- 333 27. V. Cindro *et al.*, "Radiation damage in p-type silicon irradiated with neutrons and protons," Nucl. Instr. and  
334 Meth. A 599, 60 (2009); DOI: [10.1016/j.nima.2008.11.007](https://doi.org/10.1016/j.nima.2008.11.007).
- 335 28. RD50 Collaboration, <http://rd50.web.cern.ch/rd50/>.
- 336 29. C. Jacoboni, C. Canali, G. Ottaviani and A. Alberigi Quaranta, "A review of some charge transport properties  
337 of silicon," Solid-State Electronics 20, 77 (1977); DOI: [10.1016/0038-1101\(77\)90054-5](https://doi.org/10.1016/0038-1101(77)90054-5).

338 © 2020 by the authors. Submitted to *Sensors* for possible open access publication under the terms and conditions  
339 of the Creative Commons Attribution (CC BY) license (<http://creativecommons.org/licenses/by/4.0/>).